Nanoscale Advances

Accepted Manuscript

This article can be cited before page numbers have been issued, to do this please use: D. C. Hayes, O. Z. Choudhry, S. Agarwal, K. C. Vincent, H. Belmonte and R. Agrawal, *Nanoscale Adv.*, 2025, DOI: 10.1039/D5NA00587F.

ROYAL SOCIETY OF CHEMISTRY

rsc.li/nanoscale-advances

View Article Online
DOI: 10.1039/D5NA00587F

ARTICLE

Solution-phase Synthesis and Characterization of Alkaline Earth Polysulfides as Colloidal Nanocrystals

Received 00th January 20xx,
Accepted 00th January 20xx

DOI: 10.1039/x0xx00000x

Daniel C. Hayes,[a] Omair Z. Choudhry,[a] Shubhanhsu Agarwal,[a] Kiruba Catherine Vincent,[a] Huamã Belmonte,[b] Rakesh Agrawal *[a]

Solution-chemistry fabrication of semiconductor materials are an attractive synthesis method that allows for easy post-synthesis use in various applications. In this work, we investigate the solution-phase synthesis of a lesser-studied class of semiconductor materials, the binary sulfides of the alkaline-earth (AE) metals and their potential for forming as polysulfides. Studies have shown that metal polysulfides are widely studied as cathode materials in metal-sulfur batteries and that isolatable metal polysulfides outside of solution are quite rare. Other studies have shown that this material system has the potential as wide-bandgap semiconductors or superconducting electrides and can also be used as an AES_n precursor to access certain AE-M-S ternary materials. We show that the synthesis of Ba and Sr polysulfides are strongly correlated to the reaction temperature and that the length of the S_n^{2-} oligomer chain is the dependent variable. To the best of our knowledge, we also report on the synthesis of a previously unreported polymorph of SrS_2. With bandgaps, estimated via UV-vis spectroscopy, spanning the upper energy range of the visible spectrum (2.4-3.0 eV), the AE polysulfides have potential in semiconducting applications such as displays, transparent conducting oxides, or tandem photovoltaics, just to name a few. Paired with their high crustal abundance and relative low toxicity, these materials make good candidates for future study as wide-bandgap semiconductors.

1. Introduction

Chalcogenide semiconductors are a class of materials that cover an enormous array of different compositions, properties, and applications including photovoltaics, thermoelectrics, light-emitting diodes (LEDs), and other devices which take advantage of the unique optoelectronic properties that these materials have to offer. Many iterations of chalcogenide semiconductors—from the likes of $Cu(In,Ga)(S,Se)_2$, Cu_2-II-IV-$(S,Se)_4$ (II = Sr, Ba, Zn, Cd, for example; IV = Sn or Ge for example), and II-VI and IV-VI chalcogenides (i.e. CdSe or PbS) among many others—have been extensively studied over the years and many have seen considerable success as materials for photovoltaic applications or LEDs.[1–14] For applications in which a wider band gap is desirable (i.e. as buffer layers in solar cells, transparent thin film transistors, photoelectrocatalysts for water splitting, and visible LED displays to name a few), alkaline-earth (AE)-based chalcogenides have begun to receive considerable attention in binary and other multinary materials.[15] This includes the chalcogenide perovskites,[16,17] noteworthy for having received considerable attention in the last decade for having an extremely high absorption coefficient ($>2 \times 10^5$ cm^{-1} at $E = E_g + 0.5$ eV for $BaZrS_3$)[18] and an increased, across-the-board stability over halide perovskites,[19,20] with various studies of its fundamental properties[21–25] and moderation of synthesis protocols for increased ease-of-use.[26–32] Aside from being earth-abundant, AE-based chalcogenides can also be used as alternatives to other heavy metal chalcogenides such as many of the popular II-VI and IV-VI compounds containing Cd or Pb which carry concerns related to toxicity.

Another unique property of the chalcogens is their ability to stabilize into polychalcogenide chains of various lengths (X_n^{2-}, $n \geq 2$). These polychalcogenide chains possess a unique chemical makeup and can be used to access kinetically stabilized or metastable materials, many of which may possess attractive and unusual chemical and physical properties.[33] Polysulfides in particular see extensive use in metal-sulfur batteries particularly for the Li-S system.[34] Despite the advances made in Li-S batteries recently, challenges remain such as its propensity for forming dendrites during cell operation and the anticipated cost increase and ever-limiting availability of Li. This has motivated researchers to investigate other metal-sulfur systems, including that of Mg and Ca as alternatives to Li,[35] potentially opening the door to further research into other AE-sulfur battery systems.

Over the years, the scientific community has seen an increased number of works into the AE polychalcogenides from fundamental studies on the chemical and physical properties they possess,[36–42] to their potential for applications in devices from thermoelectrics to photovoltaics and photodetectors.[43–46]

[a] Davidson School of Chemical Engineering, Purdue University, West Lafayette, IN 47907, USA
[b] Chemical Engineering, Escola Politécnica da Universidade de São Paulo, São Paulo, Brazil
† Footnotes relating to the title and/or authors should appear here.
Supplementary Information available: [details of any supplementary information available should be included here]. See DOI: 10.1039/x0xx00000x

View Article Online
DOI: 10.1039/D5NA00587F

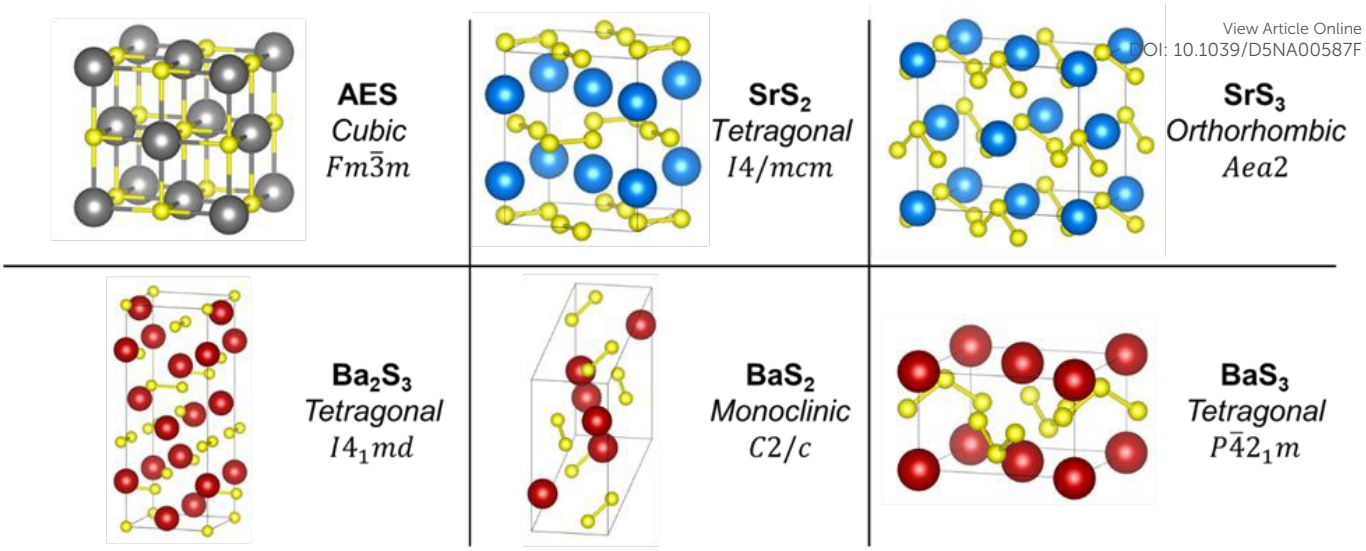

Figure 1. Shown are the unit cells of the standardized AE polysulfide crystal structures of the ICSD and the $Fm\bar{3}m$ rock salt structure of the AE monosulfides (excluding BeS). Each illustration is listed with its chemical formula, crystal system, and space group in which it belongs. Sr atoms are in blue, Ba atoms are in red, S atoms are in yellow, and any AE atom (from Mg to Ba) is in grey. The collection codes used for generating these illustrations are ICSD# 642 (SrS_2), ICSD# 23638 (SrS_3), ICSD# 70058 (Ba_2S_3), ICSD# 2004 (BaS_2), and ICSD# 70059 (BaS_3). These illustrations were generated using VESTA.[70]

Among the AE metals, polysulfides of Mg up to Ba have been reported, but crystal structures have been standardized only for those of Ba and Sr,[47] possibly owing to the difficulty in synthesizing quality and/or isolating stable samples of the lighter AE polysulfides for a detailed characterization. **Figure 1** shows the crystal structure of these standardized AE polysulfides, namely SrS_2, SrS_3, BaS_2, BaS_3, and Ba_2S_3, a non-integer polysulfide, along with the $Fm\bar{3}m$ rock salt structure of the AE monosulfides (excluding BeS which crystallizes in the $F\bar{4}3m$ zincblende structure) which are part of the Inorganic Crystal Structure Database (ICSD). Notably, the polysulfide chains containing S-S bonds can be seen in these structures with bent S_3^{2-} chains for the trisulfides. Previous work shows that the AE polysulfides BaS_2 and BaS_3 have unique chemical and electronic structures that allow for accessing more complex ternary systems via solid-state techniques at milder conditions.[40] Various methods are used to synthesize metal chalcogenides including solid state techniques, but solution-based methods—of particular interest for this work—have also been explored. Synthesis and fabrication of materials via solution methods can bypass the need for capitally-intensive and/or energy-demanding equipment (i.e. vacuum based methods like sputtering, atomic-layer deposition, or molecular beam epitaxy and/or high temperature furnaces for solid-state reactions) and additionally can allow for easy post synthesis use in deposition or thin film fabrication.[3,48–51]

In this work, we have studied the controlled formation of AE polysulfides, particularly of Ba and Sr, via solution-based methods. We have shown that the formation of these materials is highly dependent on reaction temperature, leading to polysulfides of different S_n^{2-} chain length (n = 2-3). Temperature has been known to be a key factor in dictating polychalcogenide chain length, due to the thermal instability exhibited by X_n^{2-} chains,[33] with lower temperatures containing predominantly larger n values and higher temperatures containing predominantly smaller n values.[52] In an alkylamine-sulfur system, used in our synthesis protocol, polysulfide anions are formed upon a reactive dissolution of elemental sulfur with the alkylamine, and are expected to represent one of the primary reactive sulfur species in solution.[53] If we assume a similar trend of polysulfide chain length as a function of temperature in the amine-sulfur system, it would seem that the selective synthesis of metal polysulfides of varying chain length should be possible via solution-based methods. By tuning the reaction temperature in our system, we can access BaS_2, BaS_3, and, to the best of our knowledge, a previously unreported polymorph of SrS_2 by reacting AE salts with elemental sulfur in oleylamine. We show that the chain length, n, of the synthesized AE polysulfides follows the trend of higher temperatures yielding shorter chain lengths (lower n values) down to n = 1, while lower temperatures can be used to access the polysulfides. We show that with our methods here, barium has the most control over chain length, between $2 \leq n \leq 3$, while strontium is only able to stabilize the n = 2 polysulfide. Ca was also included in this study but was found to form only as the monosulfide (CaS) regardless of the reaction conditions used during this study. In addition to the synthesis of these polysulfide materials, we also observe the absorption properties of these materials via UV-vis and assess their viability for use in optoelectronic devices.

2. Experimental Methods

2.1 Materials

Barium acetylacetonate hydrate ($Ba(acac)_2 \cdot xH_2O$) and Strontium acetylacetonate hydrate (99%, $Sr(acac)_2 \cdot xH_2O$) were purchased from Strem. Calcium acetylacetonate hydrate (99.95%, $Ca(acac)_2 \cdot xH_2O$), elemental sulfur (≥99.99% trace metals basis, S), calcium hydride (Reagent grade, 95%, CaH_2), and oleylamine (technical grade, 70%, OLA) were purchased from Sigma-Aldrich. The AE acac salts were placed in a round

View Article Online
DOI: 10.1039/D5NA00987F

bottom flask dried *in vacuo* for ~12-16 hours using Schlenk line techniques with a heating mantle set to 150 °C. The oleylamine underwent successive freeze-pump-thaw cycles followed by stirring for ~12-16 hours over CaH_2 *in vacuo* at room temperature followed by an additional 2 hours at a heating mantle setpoint of 200 °C to remove residual water while still *in vacuo*. After drying over CaH_2, the oleylamine was decanted and distilled *in vacuo* followed by storage over 3 Å molecular sieves. The S and CaH_2 were used as received.

2.2 Nanocrystal Synthesis

All material prep and post-synthesis workup was performed in an inert, N_2-filled glovebox. For the synthesis of AE sulfide nanocrystals, our standard procedure used a metal:S ratio of 1:12. In a typical synthesis, 0.25 mmol of the AE salt was combined with 3 mmol of S flakes into 3 mL of dried OLA into a borosilicate glass microwave reaction vial with a small PTFE-coated magnetic stir bar. Unless otherwise specified, the reactions were performed in a Biotage Initiator EXP or Biotage Initiator+ 400 W microwave reactor for 60 min at varying temperatures from 100 °C to 300 °C at a stir rate of 600 RPM. After the synthesis, nanocrystals were washed using a ~1:5 mixture of toluene:IPA—first adding toluene and mixing followed by IPA and mixing—and centrifuged at 14,000 RPM for 5 min. This washing procedure was repeated one additional time before storing the synthesized nanocrystals in a scintillation vial with toluene in the glovebox before further usage and characterization.

2.3 Characterization

Raman spectra were collected using a Horiba/Jobin-Yvon HR800 Raman spectrometer with a 632.8 nm wavelength excitation laser. Powder X-ray diffraction (pXRD) data were collected using a Rigaku SmartLab diffractometer with a Cu Kα (λ = 1.5406 Å) source operated at 40 kV/44 mA in parallel-beam mode. When identifying experimental pXRD data, standardized data from the Inorganic Crystal Structure Database (ICSD) was used as a reference. Elemental composition measurements were taken on a Fisher XAN 250 X-ray fluorescence (XRF) instrument at a 50 kV voltage with a silicon drift detector, primary nickel filter, and flowing helium gas purge. Transmission electron microscopy (TEM) images were taken using both a Tecnai G2 20 and Talos 200i microscopes with an accelerating voltage of 200 kV. UV-Vis diffuse reflectance data were collected from nanocrystal drop-cast films on soda-lime glass substrates using a PerkinElmer Lambda 950 spectrometer equipped with an integrating sphere. The reflectance spectra were then transformed to absorption spectra (wavelength vs absorbance) using the Kubelka-Munk function to estimate the band gap.

3. Results and Discussion

To minimize experimental complexity, our primary synthesis protocol of the AE polysulfides consisted of a simple system with only three components: a solvent/ligand (OLA), a sulfur source (elemental sulfur), and an AE source (AE acac salts). In its elemental form, sulfur can exist as many different allotropes but thermodynamically favors a crown-shaped, cyclooctasulfur (S_8) ring as its most stable form—important to consider for understanding how these polysulfides might form. The number of S units in this more stable form can consequently decrease or increase in the liquid or gaseous state caused by changes in temperature and/or pressure due to the sensitivity of polychalcogenides to changes in these variables.[33,52,54] For sulfur in solution with primary amines, the behavior and chain length of elemental sulfur is less understood, but it is known that the reactive dissolution does generate polysulfide anions via a ring-opening mechanism.[53]

Structural characterization of the polysulfide nanocrystals formed via solvothermal reactions in the microwave reactor is shown in **Figure 2** with data obtained via pXRD measurements. Data is shown for the temperature studies of the Ba-, Sr-, and Ca-S systems in the range of 130 °C to 250 °C which exemplifies the effect temperature has on polysulfide formation in alkylamine-sulfur solutions, particularly for the Ba-S and Sr-S systems. Beginning with the Ba-S system, we can see good agreement between the lower temperature products (130-160 °C) with the BaS_3 standard. When increasing the temperature above 160 °C but below 250 °C, pXRD results seem to indicate that a "region of instability" may exist preventing the formation of either of the expected Ba polysulfide species, especially for the 190 °C reaction product. Favorability towards BaS_2 can be seen at 220 °C, but it currently is not clear why this temperature region does not instead primarily show a mixture of BaS_3 and BaS_2 products. Once the reaction temperature is raised to 250 °C, there is again good agreement with previous standards—BaS_2 in this case. Additional data on reactions of the Ba-S system performed at 100 °C and 300 °C are given in **Figure S1** where we see that the reaction pressure and/or residual presence of volatile reaction byproducts can also influence the reaction product. The close match of the Ba-polysulfide spectra with the ICSD standards indicates the degree of phase purity achievable for these synthesis protocols.

Next, the Sr-S system also shows tunability for its polysulfide chain length but is shown here to exist only as the disulfide or monosulfide. SrS_3 was not obtainable as a phase-pure product via the methods explored in this work. Looking closely at the 130 °C and 160 °C reaction products, though, there is indication that it may show up as a minor product for the Sr-S reactions performed at lower temperatures. Its formation may suggest that through further optimization of reaction parameters, phase-pure SrS_3 nanocrystals may be attainable. The most notable result from the Sr-S system is the formation of, to the best of our knowledge, an unreported polymorph of SrS_2 in the range of 130 °C to 190 °C. This form of SrS_2 has structural characteristics similar to BaS_2 based on qualitative similarities in the pXRD patterns and Raman spectra (shown in **Figure 3**). A search through the ICSD and the International Centre for Diffraction Data (ICDD) reveals these databases do not contain

View Article Online
DOI: 10.1039/D5NA00587F

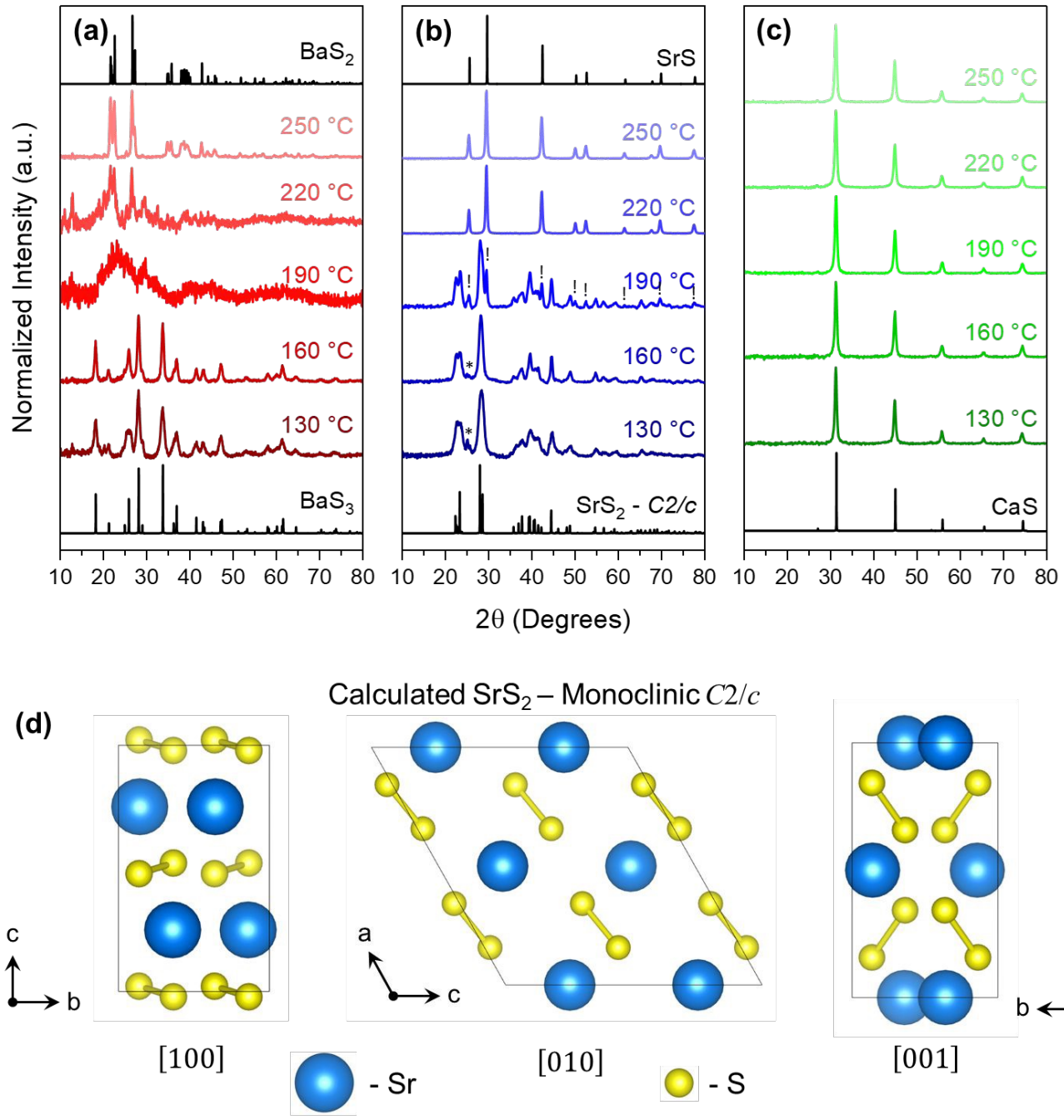

Figure 2. Temperature studies of the Ba-, Sr-, and Ca-S systems are shown for the temperature range of 130 °C to 250 °C, characterized via pXRD, in (a), (b), and (c), respectively. We attribute the peaks marked with ! and * in the Sr-S system to SrS and traces of SrS_3, respectively. The standards used in this figure are ICSD# 70059 (BaS_3), ICSD# 2004 (BaS_2), ICSD# 28900 (SrS), and ICSD# 28902 (CaS). Shown in (d) is the unit cell of the monoclinic *C*/2*c* crystal structure of SrS_2 from three different orientations, determined and optimized during Rietveld refinement of the 160 °C experimental data of the Sr-S system by adjusting the BaS_2 standard to best fit the Sr-S data. More information can be found in the supporting information in **Figure S2 and Table S1**. The crystal structure illustration in (d) was generated using VESTA.[70]

any crystal structures in the Sr-S family that are a close match to our experimental SrS_2 data. To further justify our claim that this is a new polymorph, closely related in structure to the monoclinic *C2/c* phase of BaS_2, we performed a Rietveld refinement on the experimental data using a simulated structure of SrS_2 in this same crystal motif. This result is shown in **Figure S2** and shows good agreement with the calculated structure. Some additional data on the crystal structure generated during the refinements are given in **Table S1** and comparisons between the calculated SrS_2 structure and other structures in the ICSD are also provided in **Figure S3** for the readers' reference.

Looking more closely at the Raman spectra, we see a striking similarity between that of the BaS_2 and SrS_2 nanocrystals with

View Article Online
DOI: 10.1039/D5NA00587F

the most prominent peak for both located at ~474 cm^{-1} and a similar peak shape with (at least) two overlapping signals from the stretching signal of the S_2^{2-} bonds. The Raman spectra obtained for polysulfides like these materials are dominated by the covalent bonds in the S_n^{2-} chains[36] which supports the notion that they reside in similar coordination environments and thus have a similar overall crystal structure. It should be noted that previous studies on Sr polysulfides were carried out via solid-state mechanisms. One such study conducts its synthesis at a high temperature and pressure (900 °C, 20 kbar) with SrS and elemental S to generate SrS_2 crystals.[55] Another study investigates reactions of $Sr(OH)_2$ with elemental sulfur at relatively low temperatures (200 °C), presumably at atmospheric pressures under a flow of N_2 gas (though the study does not make it entirely clear), to form SrS_3 followed by decomposition at 300 °C, breaking down the S_3^{2-} chains, to generate SrS_2.[56] These studies may indicate that either high pressures are needed to fabricate polysulfides of Sr, or that certain precursors (i.e. $Sr(OH)_2$) may be needed to provide a kinetic pathway for the formation of Sr polysulfides. For the reactions starting at 190 °C and higher, we begin to see the formation of SrS alongside SrS_2 for 190 °C, and phase-pure SrS for 220 °C and higher.

In addition to the structural characterizations shown thus far, XRF measurements revealed a Ba:S ratio of ~1:3 and ~1:2 for the BaS_3 and BaS_2 products, respectively, and a Sr:S ratio of ~1:2 for the SrS_2 product. Plots of these data can be seen in **Figure S4**. The Ca-S system was also studied for its potential to form polysulfides via solution-phase methods. As stated previously, this material system has been used in Ca-S batteries[35] and also predicted to have some interesting electronic properties as superconducting electrides but so far has only been computationally predicted and experimentally isolated as polysulfides under high pressures.[37,43] Over the entire temperature range used in this study (130-250 °C), only the monosulfide, CaS, was found to form. Powder XRD characterization data for the Ca-S experiments are also shown in **Figure 2c** with additional analysis of the pXRD data in **Figure S5**. Here, it is shown that the growth and ultimate size of the CaS nanocrystals is not particularly sensitive to changes in temperature (at least given the conditions and temperature range investigated here), suggesting that given the precursor choices in this study, nucleation and growth occurs quite rapidly. The general sharpness of the pXRD peaks further corroborates this claim.

Based on these results, the polysulfide anion chain length in the isolated crystal structure is not solely temperature dependent as the AE cation is also shown to affect the chain length of the isolated product. Under our reaction conditions at 160 °C, for example, the majority product with Ba, Sr, and Ca is with n = 3, 2, and 1, respectively. One might consider cation size to play a prominent role, but considering another example in PbS nanocrystals, it is shown that with the use of sulfur-oleylamine solutions at temperatures as low as 40 °C, only the monosulfide of Pb forms.[57] The ionic radii of Pb^{2+} is comparable to Ba^{2+} and Sr^{2+} (in pm, 133, 149, and 132, respectively) indicating that there are likely other contributing factors. This

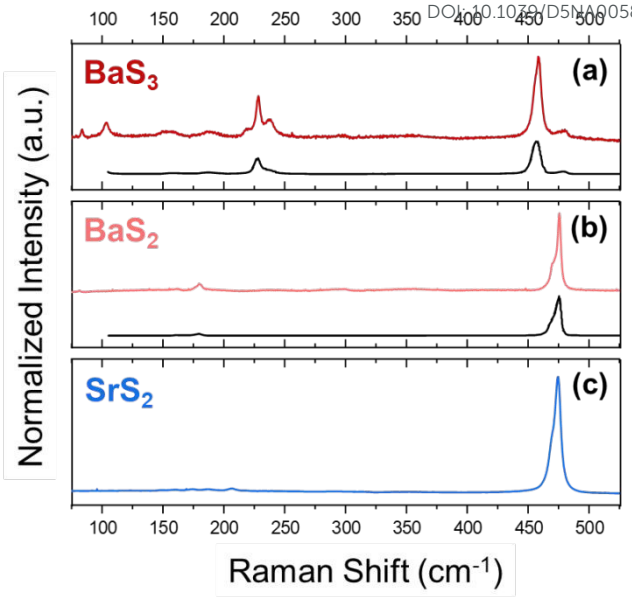

Figure 3. Raman spectroscopy of the alkaline-earth polysulfide samples of BaS_3 (a), BaS_2 (b), and SrS_2 (c), at 160 °C, 250 °C, and 160 °C, respectively, in the microwave reactor. The plots in black at the bottom of (a) and (b) were digitized from Sasaki et al. and are used for visual comparison of BaS_3 and BaS_2, respectively, to previously reported work.[40]

phenomenon likely stems from the relatively unstable thermodynamics and (due to their similar Gibbs free energies) the complex disproportionation/comproportionation equilibria present with polysulfide anions of different n values resulting in very few metal polysulfides reported to be isolatable outside of mixtures with excess sulfur.[34,58] Various techniques exist to characterize polysulfide species,[58] but the complex equilibria of these polysulfides makes it quite difficult to characterize individual species and is beyond the scope of this work.

TEM data are shown in **Figure 4** and **Figures S6-S7** for the three species with both low-resolution and high-resolution images, respectively, for gauging size dispersity and observing crystal planes of the nanocrystals. Indicated by the general sharpness of the pXRD data (**Figure 2**) and shown in the TEM images (**Figure 4**), we can see that nanocrystal sizes are on the order of (at least) several tens of nanometers. Nanocrystal size can play a big role in the colloidal stability of nanomaterials by overcoming Brownian motion in solution once the nanocrystals

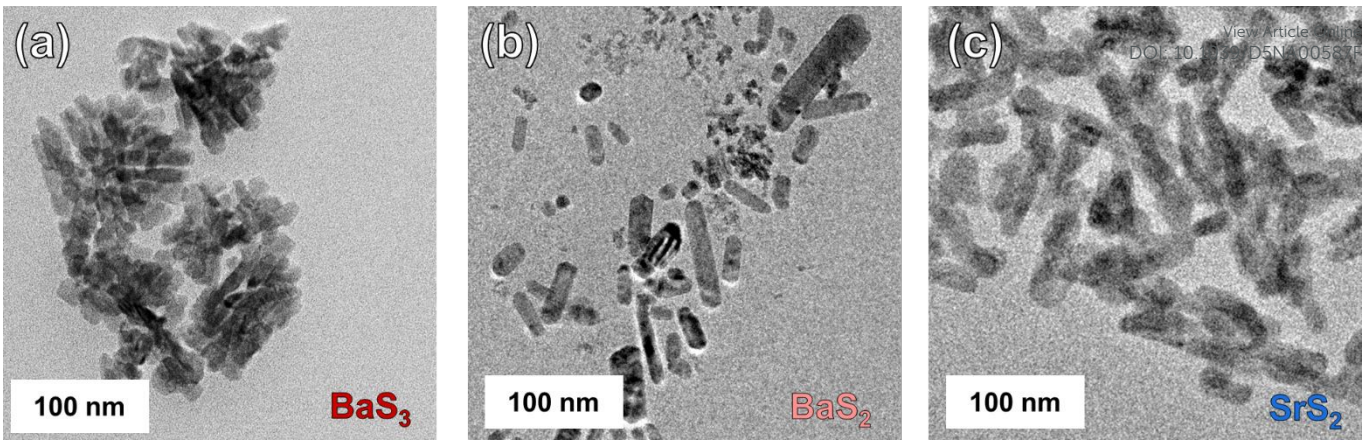

Figure 4. TEM images of the BaS_3, BaS_2, and SrS_2 nanocrystals are shown in (a), (b), and (c), respectively. These nanocrystals were synthesized at 160 °C, 250 °C, and 160 °C in a sealed microwave vessel for BaS_3, BaS_2, and SrS_2, respectively. The nanocrystals synthesized in this study appear to all resemble shape anisotropy with rod-like structures.

surpass a critical size. As such, we at least partially associate the observation that these nanocrystals settle out of solution after only a few minutes of resting due to these larger crystal sizes. Another possible large contribution is the surface functionality of the synthesized nanocrystals which dictates ligand coverage and aggregation potential. OLA, as it was used in this protocol, is widely used in a variety of nanocrystal syntheses as a stabilizing ligand for generating colloidally stable nanomaterials. In the case of these materials, it seems as though OLA alone is not sufficient for adequately stabilizing these materials. This may be due to a lower binding affinity of the -NH_2 functional group to the surfaces of the AE polysulfides.

Apart from this discussion on surface functionality, we can see that each nanocrystal species presents a moderate degree of shape anisotropy. All species appear to have somewhat similar rod-like morphologies with BaS_3 appearing to form as feather- or fan-like clusters. Further work with these synthesis protocols, including experimentation with different ligands (i.e. carboxylic acids, phosphines, thiols, etc.) and different precursors (though care should be taken to avoid insoluble AE precursors or less reactive precursors such as the AE halides[59]) would be needed to synthesize more colloidally stable nanocrystals—important for downstream usage for homogeneous inks and/or coatings. More discussion on precursor choices is given in **Figure S8** along with the supplementary discussion that follows.

To our knowledge, only one report thus far has been reported for the band structure of any of the compounds synthesized in this work—specifically, monoclinic BaS_2—via density functional theory calculations using the generalized gradient approximation with the PW91 exchange-correlation (XC) functional.[46] In this previous work, BaS_2 is predicted to have an indirect bandgap of 1.535 eV and a direct bandgap transition at a slightly higher energy. The PW91 functional tends to underestimate the bandgap of semiconductor materials as opposed to more reliable XC functionals for band structure analysis like the HSE06 or mBJ functionals[60–64] which may explain the deviation from the theoretical data to our experimental data. The experimental bandgaps were estimated using the Tauc method $(\alpha \cdot h\nu)^{1/\gamma} = B(h\nu - E_g)$ where γ = 1/2 for direct and 2 for indirect bandgaps. Since we performed reflectance measurements, the Kubelka-Munk function, $F(R)$, is applied in place of the absorption, α.[65] The literature on the bandgap of these materials is limited, so we have reported both direct and indirect band gaps in **Figure 5.** The data presented has been normalized to the maximum of $[F(R) \cdot h\nu]^{1/\gamma}$ in the window shown so that the shape and position relative to energy of each curve can be compared with one another. For all three species, we see a significant absorption onset characterizing the bandgap of each material. BaS_3 and SrS_2 have similar bandgaps of around 2.5-2.7 eV while BaS_2 has the highest bandgap of these three materials approaching 3 eV for a direct bandgap estimation. A bandgap increase from BaS_3 to BaS_2 is arguably as expected considering the band gap for BaS is reported to be between 3.5-3.9 eV.[42] Additionally, BaS_3 appears to show a second absorption event at higher energies, possibly due to a separate energy transition requiring energies slightly higher than the main energy transition. Raw data of these measurements plotted as % reflectance vs. wavelength is also provided in **Figure S9**.

We should also note that in their native state, these materials did not show any distinct photoluminescence (PL) when cast as a film. If we assume these are direct bandgap materials, this could possibly be indicative of a defective material, but in nanocrystals, deleterious surface states must also be considered for the lack of notable PL. Since the properties of nanocrystals are largely dominated by their surfaces, an accumulation of harmful surface defects caused by dangling bonds from improper or incomplete surface passivation can easily quench any PL signal.[66] This can be addressed by fabricating core-shell nanocrystal structures where the material of interest resides in the core, and a passivating shell is formed around the core to promote increased PL yields.[67] Additionally, ligand exchange procedures can be used to replace the native ligands from the nanocrystal synthesis with a ligand(s) better suited to passivate harmful surface defects.

4. Conclusions

View Article Online
DOI: 10.1039/D5NA00587F

The earth-abundant, AE polysulfides are a lesser studied class of materials but are predicted to have some interesting attributes making them attractive for semiconducting applications. This study covers the solution-based synthesis of three different AE polysulfide nanocrystals (BaS_3, BaS_2, and SrS_2) via colloidal methods by the variation of one key parameter—the reaction temperature. Given a heavier AE metal (Ba or Sr), changing the reaction temperature allows us to fine tune the chain length of the S_n^{2-} chains leading to the different species discussed. In addition to the synthesis of the Ba polysulfides, we discuss the formation of, to the best of our knowledge, an unreported polymorph of SrS_2 which is different from that in the Inorganic Crystal Structure Database for SrS_2. We then assess some of the basic absorption properties of these materials via UV-vis measurements and find that their bandgaps fall within what would typically consider these materials as wide-bandgap semiconductors.

Considering the instabilities of the polysulfides and the protocols in this study unable to stabilize certain, phase-pure polysulfide species ($n > 2$ for Sr, $n > 1$ for Ca, and other non-integer values of n such as with Ba_2S_3), it should be recalled that solution-based nanomaterials have the ability to access metastable phases as a result of non-equilibrium reaction kinetics and the influence of surface energies on the system thermodynamics. Additionally, cation-exchange methods have often been performed to access metastable polymorphs of various materials.[68,69] With this in mind, with the right precursors, solvents, ligands, and other reaction parameters, stabilization of these additional phases may be possible. Further work also remains to increase the colloidal stability of these materials, as flocculation observed when handling the samples suggests aggregation in their native form. Additionally, photoluminescence of these materials was not observed; however, surface modifications including, but not limited to, core-shell structures and/or ligand exchange methods—not investigated in this study—should be explored to assess if deleterious surface states are responsible for the lack of notable photoluminescence. Furthermore, pairing experiments such as these with detailed computational studies on the band structures of these materials would help to get a more thorough idea of their optoelectronic properties. We hope that by expanding the catalogue of synthesizable nanocrystals, this work allows others to explore AE polysulfide nanocrystals and the potential applications that may await these materials.

Author contributions

DCH: conceptualization, data curation, formal analysis, investigation, methodology, visualization, writing – original draft, writing – review & editing. OC: data curation, formal analysis, investigation, validation. SA: data curation, investigation, validation, writing – review & editing. KCV: data curation, writing – review & editing. HB: data curation, investigation. RA: funding acquisition, supervision, writing – review & editing.

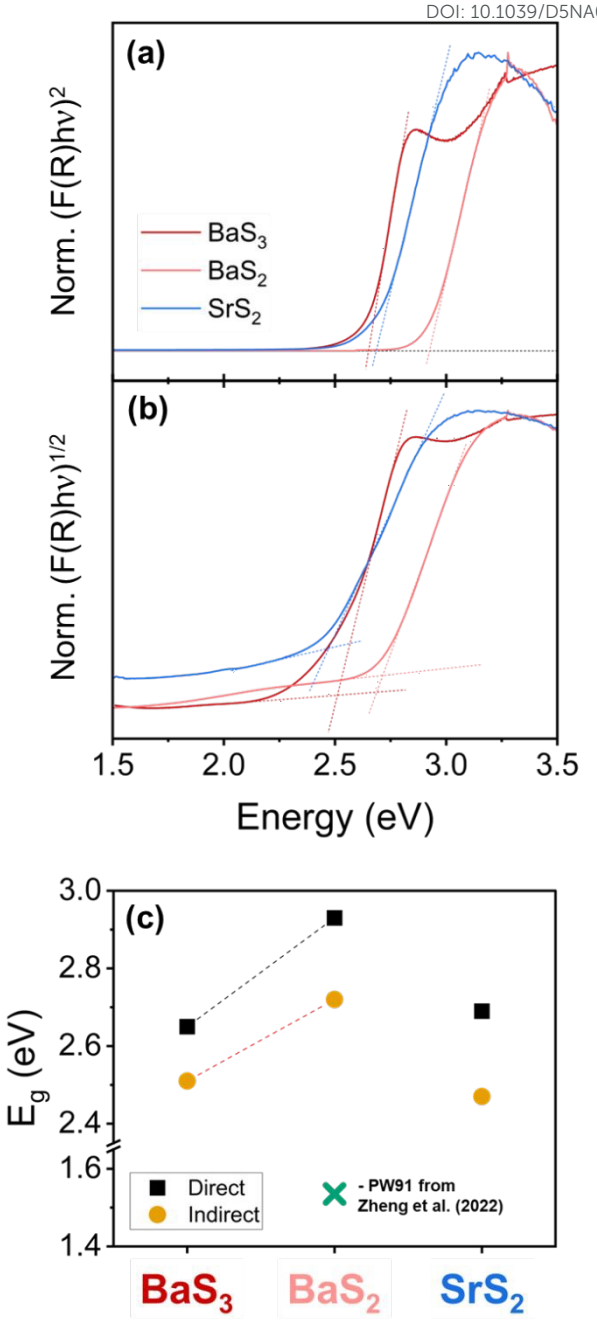

Figure 5. Kubelka-Munk transformations used to determine the bandgap of the synthesized nanocrystals. The direct transformation is shown in (a), and the indirect transformation is shown in (b). (c) displays the bandgaps determined from these measurements with the direct and indirect energy gaps of BaS_3, BaS_2, and SrS_2 being 2.65, 2.51; 2.93, 2.72; and 2.69, 2.47 eV, respectively. The blue cross in (c) represents the calculated data from the computational study on Ba dichalcogenides.[46] These measurements were performed on nanocrystals synthesized at 160 °C, 250 °C, and 160 °C for BaS_3, BaS_2, and SrS_2, respectively.

Conflicts of interest

There are no conflicts to declare.

View Article Online
DOI: 10.1039/D5NA00587F

Data availability

Additional data supporting the results in this article have been included as part of the ESI which includes additional pXRD data, XRF data, and TEM data, followed by a short supplementary discussion on precursor choices.

Acknowledgements

The authors are grateful for the financial support from the National Science Foundation through grants 1735282-NRT (SFEWS) and 1855882 (INFEWS). We would also like to thank Dr. Matthias Zeller for his help in performing the Rietveld refinement and determining a crystal structure match for the new SrS_2 polymorph. A special thanks is also given to Dr. Jonathan W. Turnley for his fruitful discussions in the early stages of this project.

References

(1) Scarpulla, M. A.; McCandless, B.; Phillips, A. B.; Yan, Y.; Heben, M. J.; Wolden, C.; Xiong, G.; Metzger, W. K.; Mao, D.; Krasikov, D.; Sankin, I.; Grover, S.; Munshi, A.; Sampath, W.; Sites, J. R.; Bothwell, A.; Albin, D.; Reese, M. O.; Romeo, A.; Nardone, M.; Klie, R.; Walls, J. M.; Fiducia, T.; Abbas, A.; Hayes, S. M. CdTe-Based Thin Film Photovoltaics: Recent Advances, Current Challenges and Future Prospects. *Solar Energy Materials and Solar Cells* **2023**, *255*, 112289. https://doi.org/10.1016/j.solmat.2023.112289.

(2) Brown, P. R.; Kim, D.; Lunt, R. R.; Zhao, N.; Bawendi, M. G.; Grossman, J. C.; Bulović, V. Energy Level Modification in Lead Sulfide Quantum Dot Thin Films through Ligand Exchange. *ACS Nano* **2014**, *8* (6), 5863–5872. https://doi.org/10.1021/nn500897c.

(3) Suresh, S.; Uhl, A. R. Present Status of Solution-Processing Routes for Cu(In,Ga)(S,Se) 2 Solar Cell Absorbers. *Adv Energy Mater* **2021**, *11* (14), 2003743. https://doi.org/10.1002/aenm.202003743.

(4) Hadke, S.; Huang, M.; Chen, C.; Tay, Y. F.; Chen, S.; Tang, J.; Wong, L. Emerging Chalcogenide Thin Films for Solar Energy Harvesting Devices. *Chem Rev* **2022**, *122* (11), 10170–10265. https://doi.org/10.1021/acs.chemrev.1c00301.

(5) Lie, S.; Guc, M.; Tunuguntla, V.; Izquierdo-Roca, V.; Siebentritt, S.; Wong, L. H. Comprehensive Physicochemical and Photovoltaic Analysis of Different Zn Substitutes (Mn, Mg, Fe, Ni, Co, Ba, Sr) in CZTS-Inspired Thin Film Solar Cells. *J Mater Chem A Mater* **2022**, *10* (16), 9137–9149. https://doi.org/10.1039/D2TA00225F.

(6) Teymur, B.; Kim, Y.; Huang, J.; Sun, K.; Hao, X.; Mitzi, D. B. Top Stack Optimization for Cu 2 BaSn(S, Se) 4 Photovoltaic Cell Leads to Improved Device Power Conversion Efficiency beyond 6%. *Adv Energy Mater* **2022**, *12* (40). https://doi.org/10.1002/aenm.202201602.

(7) Wang, A.; He, M.; Green, M. A.; Sun, K.; Hao, X. A Critical Review on the Progress of Kesterite Solar Cells: Current Strategies and Insights. *Adv Energy Mater* **2023**, *13* (2). https://doi.org/10.1002/aenm.202203046.

(8) Keller, J.; Kiselman, K.; Donzel-Gargand, O.; Martin, N. M.; Babucci, M.; Lundberg, O.; Wallin, E.; Stolt, L.; Edoff, M. High-Concentration Silver Alloying and Steep Back-Contact Gallium Grading Enabling Copper Indium Gallium Selenide Solar Cell with 23.6% Efficiency. *Nat Energy* **2024**, *9* (4), 467–478. https://doi.org/10.1038/s41560-024-01472-3.

(9) Ramanujam, J.; Singh, U. P. Copper Indium Gallium Selenide Based Solar Cells – a Review. *Energy Environ Sci* **2017**, *10* (6), 1306–1319. https://doi.org/10.1039/C7EE00826K.

(10) Böhm, M. L.; Jellicoe, T. C.; Tabachnyk, M.; Davis, N. J. L. K.; Wisnivesky-Rocca-Rivarola, F.; Ducati, C.; Ehrler, B.; Bakulin, A. A.; Greenham, N. C. Lead Telluride Quantum Dot Solar Cells Displaying External Quantum Efficiencies Exceeding 120%. *Nano Lett* **2015**, *15* (12), 7987–7993. https://doi.org/10.1021/acs.nanolett.5b03161.

(11) Ahmad, W.; He, J.; Liu, Z.; Xu, K.; Chen, Z.; Yang, X.; Li, D.; Xia, Y.; Zhang, J.; Chen, C. Lead

Selenide (PbSe) Colloidal Quantum Dot Solar Cells with >10% Efficiency. *Advanced Materials* **2019**, *31* (33). https://doi.org/10.1002/adma.201900593.

(12) Crovetto, A.; Xing, Z.; Fischer, M.; Nielsen, R.; Savory, C. N.; Rindzevicius, T.; Stenger, N.; Scanlon, D. O.; Chorkendorff, I.; Vesborg, P. C. K. Experimental and First-Principles Spectroscopy of Cu 2 SrSnS 4 and Cu 2 BaSnS 4 Photoabsorbers. *ACS Appl Mater Interfaces* **2020**, *12* (45), 50446–50454. https://doi.org/10.1021/acsami.0c14578.

(13) Rogach, A. L.; Gaponik, N.; Lupton, J. M.; Bertoni, C.; Gallardo, D. E.; Dunn, S.; Li Pira, N.; Paderi, M.; Repetto, P.; Romanov, S. G.; O'Dwyer, C.; Sotomayor Torres, C. M.; Eychmüller, A. Light-Emitting Diodes with Semiconductor Nanocrystals. *Angewandte Chemie International Edition* **2008**, *47* (35), 6538–6549. https://doi.org/10.1002/anie.200705109.

(14) Turnley, J. W.; Agrawal, R. Solution Processed Metal Chalcogenide Semiconductors for Inorganic Thin Film Photovoltaics. *Chemical Communications* **2024**, *60* (40), 5245–5269. https://doi.org/10.1039/D4CC01057D.

(15) Woods-Robinson, R.; Han, Y.; Zhang, H.; Ablekim, T.; Khan, I.; Persson, K. A.; Zakutayev, A. Wide Band Gap Chalcogenide Semiconductors. *Chem Rev* **2020**, *120* (9), 4007–4055. https://doi.org/10.1021/acs.chemrev.9b00600.

(16) Sopiha, K. V; Comparotto, C.; Márquez, J. A.; Scragg, J. J. S. Chalcogenide Perovskites: Tantalizing Prospects, Challenging Materials. *Adv Opt Mater* **2022**, *10* (3), 2101704. https://doi.org/10.1002/adom.202101704.

(17) Agarwal, S.; Vincent, K. C.; Agrawal, R. From Synthesis to Application: A Review of BaZrS3 Chalcogenide Perovskites. *Nanoscale*. Royal Society of Chemistry January 15, 2025. https://doi.org/10.1039/d4nr03880k.

(18) Nishigaki, Y.; Nagai, T.; Nishiwaki, M.; Aizawa, T.; Kozawa, M.; Hanzawa, K.; Kato, Y.; Sai, H.; Hiramatsu, H.; Hosono, H.; Fujiwara, H. Extraordinary Strong Band-Edge Absorption in Distorted Chalcogenide Perovskites. *Solar RRL* **2020**, *4* (5), 1–8. https://doi.org/10.1002/solr.201900555.

(19) Niu, S.; Milam-Guerrero, J.; Zhou, Y.; Ye, K.; Zhao, B.; Melot, B. C.; Ravichandran, J. Thermal Stability Study of Transition Metal Perovskite Sulfides. *J Mater Res* **2018**, *33* (24), 4135–4143. https://doi.org/10.1557/jmr.2018.419.

(20) Gupta, T.; Ghoshal, D.; Yoshimura, A.; Basu, S.; Chow, P. K.; Lakhnot, A. S.; Pandey, J.; Warrender, J. M.; Efstathiadis, H.; Soni, A.; Osei-Agyemang, E.; Balasubramanian, G.; Zhang, S.; Shi, S.; Lu, T.; Meunier, V.; Koratkar, N. An Environmentally Stable and Lead-Free Chalcogenide Perovskite. *Adv Funct Mater* **2020**, *30* (23). https://doi.org/10.1002/adfm.202001387.

(21) Niu, S.; Huyan, H.; Liu, Y.; Yeung, M.; Ye, K.; Blankemeier, L.; Orvis, T.; Sarkar, D.; Singh, D. J.; Kapadia, R.; Ravichandran, J. Bandgap Control via Structural and Chemical Tuning of Transition Metal Perovskite Chalcogenides. *Advanced Materials* **2017**, *29* (9), 1604733. https://doi.org/10.1002/adma.201604733.

(22) Sadeghi, I.; Ye, K.; Xu, M.; Li, Y.; LeBeau, J. M.; Jaramillo, R. Making $BaZrS_3$ Chalcogenide Perovskite Thin Films by Molecular Beam Epitaxy. *Adv Funct Mater* **2021**, *31* (45). https://doi.org/10.1002/adfm.202105563.

(23) Sadeghi, I.; Van Sambeek, J.; Simonian, T.; Xu, M.; Ye, K.; Cai, T.; Nicolosi, V.; LeBeau, J. M.; Jaramillo, R. Expanding the Perovskite Periodic Table to Include Chalcogenide Alloys with Tunable Band Gap Spanning 1.5–1.9 EV. *Adv*

Funct Mater **2023**, *33* (41). https://doi.org/10.1002/adfm.202304575.

(24) Comparotto, C.; Davydova, A.; Ericson, T.; Riekehr, L.; Moro, M. V; Kubart, T.; Scragg, J. Chalcogenide Perovskite BaZrS 3 : Thin Film Growth by Sputtering and Rapid Thermal Processing. *ACS Appl Energy Mater* **2020**, *3* (3), 2762–2770. https://doi.org/10.1021/acsaem.9b02428.

(25) Mukherjee, S.; Riva, S.; Comparotto, C.; Johansson, F. O. L.; Man, G. J.; Phuyal, D.; Simonov, K. A.; Just, J.; Klementiev, K.; Butorin, S. M.; Scragg, J. J. S.; Rensmo, H. Interplay between Growth Mechanism, Materials Chemistry, and Band Gap Characteristics in Sputtered Thin Films of Chalcogenide Perovskite BaZrS 3. *ACS Appl Energy Mater* **2023**, *6* (22), 11642–11653. https://doi.org/10.1021/acsaem.3c02075.

(26) Vincent, K. C.; Agarwal, S.; Fan, Z.; Canizales, A. S. M.; Agrawal, R. Expanding the Horizons for Viable Precursors and Liquid Fluxes for the Synthesis of BaZrS 3 and Related Compounds. *J Mater Chem C Mater* **2024**, *12* (32), 12521–12534. https://doi.org/10.1039/D4TC02287D.

(27) Hayes, D. C.; Agarwal, S.; Vincent, K. C.; Aimiuwu, I. M.; Pradhan, A. A.; Uible, M. C.; Bart, S. C.; Agrawal, R. A Reliable, Colloidal Synthesis Method of the Orthorhombic Chalcogenide Perovskite, BaZrS 3 , and Related ABS 3 Nanomaterials (A = Sr, Ba; B = Ti, Zr, Hf): A Step Forward for Earth-Abundant, Functional Materials. *Chem Sci* **2025**, *16* (3), 1308–1320. https://doi.org/10.1039/D4SC06116K.

(28) Agarwal, S.; Vincent, K. C.; Turnley, J. W.; Hayes, D. C.; Uible, M. C.; Durán, I.; Canizales, A. S. M.; Khandelwal, S.; Panicker, I.; Andoh, Z.; Spilker, R. M.; Ma, Q.; Huang, L.; Hwang, S.; Kisslinger, K.; Svatek, S.; Antolin, E.; Bart, S. C.; Agrawal, R. Breaking Barriers in Chalcogenide Perovskite Synthesis: A Generalized Framework for Fabrication of BaMS 3 (M═Ti, Zr, Hf) Materials. *Adv Funct Mater* **2024**, *34* (46). https://doi.org/10.1002/adfm.202405416.

(29) Yang, R.; Jess, A. D.; Fai, C.; Hages, C. J. Low-Temperature, Solution-Based Synthesis of Luminescent Chalcogenide Perovskite BaZrS 3 Nanoparticles. *J Am Chem Soc* **2022**, *144* (35), 15928–15931. https://doi.org/10.1021/jacs.2c06168.

(30) Yang, R.; Nelson, J.; Fai, C.; Yetkin, H. A.; Werner, C.; Tervil, M.; Jess, A. D.; Dale, P. J.; Hages, C. J. A Low-Temperature Growth Mechanism for Chalcogenide Perovskites. *Chemistry of Materials* **2023**, *35* (12), 4743–4750. https://doi.org/10.1021/acs.chemmater.3c00494.

(31) Comparotto, C.; Ström, P.; Donzel-Gargand, O.; Kubart, T.; Scragg, J. J. S. Synthesis of BaZrS 3 Perovskite Thin Films at a Moderate Temperature on Conductive Substrates. *ACS Appl Energy Mater* **2022**, *5* (5), 6335–6343. https://doi.org/10.1021/acsaem.2c00704.

(32) Zilevu, D.; Parks, O. O.; Creutz, S. E. Solution-Phase Synthesis of the Chalcogenide Perovskite Barium Zirconium Sulfide as Colloidal Nanomaterials. *Chemical Communications* **2022**, *58* (75), 10512–10515. https://doi.org/10.1039/D2CC03494H.

(33) Kanatzidis, M. G. Molten Alkali-Metal Polychalcogenides as Reagents and Solvents for the Synthesis of New Chalcogenide Materials. *Chemistry of Materials* **1990**, *2* (4), 353–363. https://doi.org/10.1021/cm00010a009.

(34) Li, G.; Wang, S.; Zhang, Y.; Li, M.; Chen, Z.; Lu, J. Revisiting the Role of Polysulfides in Lithium–Sulfur Batteries. *Advanced Materials*. Wiley-VCH Verlag May 29, 2018. https://doi.org/10.1002/adma.201705590.

(35) Chung, S. H.; Manthiram, A. Current Status and Future Prospects of Metal–Sulfur Batteries. *Advanced Materials*. Wiley-VCH Verlag July 5, 2019. https://doi.org/10.1002/adma.201901125.

(36) Eysel, H. H.; Siebert, H.; Agiorgitis, G. Raman - Spektren von Disulfiden $Me^{II}S_2$. *Zeitschrift für Naturforschung B* **1969**, *24* (7), 932–933. https://doi.org/10.1515/znb-1969-0726.

(37) Wang, S.; Lu, W.; Liu, S.; Zhou, M.; Gao, P.; Wang, H.; Lv, J.; Gou, H.; Liu, G.; Liu, H.; Wang, Y.; Ma, Y. Synthesis of Calcium Polysulfides at High Pressures. *Phys Rev B* **2021**, *104* (5), 054117. https://doi.org/10.1103/PhysRevB.104.054117.

(38) Fukuoka, H.; Suga, R.; Komaguchi, K.; Yamanaka, S.; Shiotani, M. New Strontium Polysulfides, SrS 3 , and Sr 2 (OH) 2 S 4 ·10H 2 O, Obtained by the High-Pressure Treatment of a Sr−S Mixture. *Inorg Chem* **2004**, *43* (18), 5780–5784. https://doi.org/10.1021/ic0494612.

(39) Bhutani, A.; Schiller, J. A.; Zuo, J. L.; Eckstein, J. N.; Greene, L. H.; Chaudhuri, S.; Shoemaker, D. P. Combined Computational and in Situ Experimental Search for Phases in an Open Ternary System, Ba–Ru–S. *Chemistry of Materials* **2017**, *29* (14), 5841–5849. https://doi.org/10.1021/acs.chemmater.7b00809.

(40) Sasaki, S.; Lesault, M.; Grange, E.; Janod, E.; Corraze, B.; Cadars, S.; Caldes, M. T.; Guillot-Deudon, C.; Jobic, S.; Cario, L. Unexplored Reactivity of (S n) 2− Oligomers with Transition Metals in Low-Temperature Solid-State Reactions. *Chemical Communications* **2019**, *55* (44), 6189–6192. https://doi.org/10.1039/C9CC01338E.

(41) Martin, T. P.; Schaber, H. Matrix Isolated II-VI Molecules: Sulfides of Mg, Ca, Sr, Zn and Cd. *Spectrochim Acta A* **1982**, *38* (6), 655–660. https://doi.org/10.1016/0584-8539(82)80086-X.

(42) Roth, A. N.; Chen, Y.; Adamson, M. A. S.; Gi, E.; Wagner, M.; Rossini, A. J.; Vela, J. Alkaline-Earth Chalcogenide Nanocrystals: Solution-Phase Synthesis, Surface Chemistry, and Stability. *ACS Nano* **2022**, *16* (8), 12024–12035. https://doi.org/10.1021/acsnano.2c02116.

(43) Liu, Y.-X.; Wang, C.; Han, S.; Chen, X.; Sun, H.-R.; Liu, X.-B. Novel Superconducting Electrides in Ca–S System under High Pressures. *Chinese Physics Letters* **2021**, *38* (3), 036201. https://doi.org/10.1088/0256-307X/38/3/036201.

(44) Jia, T.; Feng, Z.; Guo, S.; Zhang, X.; Zhang, Y. Screening Promising Thermoelectric Materials in Binary Chalcogenides through High-Throughput Computations. *ACS Appl Mater Interfaces* **2020**, *12* (10), 11852–11864. https://doi.org/10.1021/acsami.9b23297.

(45) Uğur, Ş.; Güler, E.; Güler, M.; Özdemir, A.; Uğur, G. Analyzing the Electronic and Optical Properties of Bulk, Unstrained, and Strained Monolayers of SrS2 by DFT. *Physica E Low Dimens Syst Nanostruct* **2022**, *143* (May), 115403. https://doi.org/10.1016/j.physe.2022.115403.

(46) Zheng, W.; Liu, F.-S.; Lu, Y.; Liu, Z.-T.; Liu, W.-H.; Liu, Q. First-Principles Calculations of the Structural, Mechanical, Electronic, and Optical Properties of BaX2 (X=O, S, Se and Te) Compounds. *Mater Sci Semicond Process* **2022**, *147* (May), 106755. https://doi.org/10.1016/j.mssp.2022.106755.

(47) Bergerhoff, G.; Hundt, R.; Sievers, R.; Brown, I. D. The Inorganic Crystal Structure Data Base. *J Chem Inf Comput Sci* **1983**, *23* (2), 66–69. https://doi.org/10.1021/ci00038a003.

(48) Pasquarelli, R. M.; Ginley, D. S.; O'Hayre, R. Solution Processing of Transparent Conductors:

From Flask to Film. *Chem Soc Rev* **2011**, *40* (11), 5406. https://doi.org/10.1039/c1cs15065k.

(49) Kagan, C. R.; Lifshitz, E.; Sargent, E. H.; Talapin, D. V. Building Devices from Colloidal Quantum Dots. *Science (1979)* **2016**, *353* (6302). https://doi.org/10.1126/science.aac5523.

(50) Carey, G. H.; Abdelhady, A. L.; Ning, Z.; Thon, S. M.; Bakr, O. M.; Sargent, E. H. Colloidal Quantum Dot Solar Cells. *Chem Rev* **2015**, *115* (23), 12732–12763. https://doi.org/10.1021/acs.chemrev.5b00063.

(51) Manser, J. S.; Saidaminov, M. I.; Christians, J. A.; Bakr, O. M.; Kamat, P. V. Making and Breaking of Lead Halide Perovskites. *Acc Chem Res* **2016**, *49* (2), 330–338. https://doi.org/10.1021/acs.accounts.5b00455.

(52) Meyer, B. Elemental Sulfur. *Chem Rev* **1976**, *76* (3), 367–388. https://doi.org/10.1021/cr60301a003.

(53) Thomson, J. W.; Nagashima, K.; Macdonald, P. M.; Ozin, G. A. From Sulfur−Amine Solutions to Metal Sulfide Nanocrystals: Peering into the Oleylamine−Sulfur Black Box. *J Am Chem Soc* **2011**, *133* (13), 5036–5041. https://doi.org/10.1021/ja1109997.

(54) Kayastha, P.; Longo, G.; Whalley, L. D. A First-Principles Thermodynamic Model for the Ba–Zr–S System in Equilibrium with Sulfur Vapor. *ACS Appl Energy Mater* **2024**. https://doi.org/10.1021/acsaem.3c03208.

(55) Kawada, I.; Kato, K.; Yamaoka, S. Strontium Disulphide Prepared at High Pressure. *Acta Crystallogr B* **1976**, *32* (11), 3110–3111. https://doi.org/10.1107/S0567740876009679.

(56) v. Schnering, H. G.; Goh, N.-K. Die Strukturen Der Polysulfide BaS3, SrS3, BaS2 Und SrS2. *Naturwissenschaften* **1974**, *61* (6), 272–272. https://doi.org/10.1007/BF00595664.

(57) Weidman, M. C.; Beck, M. E.; Hoffman, R. S.; Prins, F.; Tisdale, W. A. Monodisperse, Air-Stable PbS Nanocrystals via Precursor Stoichiometry Control. *ACS Nano* **2014**, *8* (6), 6363–6371. https://doi.org/10.1021/nn5018654.

(58) Li, X. Y.; Zhao, M.; Song, Y. W.; Bi, C. X.; Li, Z.; Chen, Z. X.; Zhang, X. Q.; Li, B. Q.; Huang, J. Q. Polysulfide Chemistry in Metal-Sulfur Batteries. *Chemical Society Reviews*. Royal Society of Chemistry April 1, 2025, pp 4822–4873. https://doi.org/10.1039/d4cs00318g.

(59) Agarwal, S.; Vincent, K. C.; Agrawal, R. Quantitative Scales for Haliphilicity of Metals: Tailoring the Halide Affinity of Alkaline Earth Metals to Synthesize Chalcogenide Perovskite BaMS 3 (M = Zr, and Hf) and Cu 2 BaSnS 4 Compounds. *ACS Appl Energy Mater* **2024**, *7* (22), 10584–10595. https://doi.org/10.1021/acsaem.4c02205.

(60) Borlido, P.; Aull, T.; Huran, A. W.; Tran, F.; Marques, M. A. L.; Botti, S. Large-Scale Benchmark of Exchange–Correlation Functionals for the Determination of Electronic Band Gaps of Solids. *J Chem Theory Comput* **2019**, *15* (9), 5069–5079. https://doi.org/10.1021/acs.jctc.9b00322.

(61) Tran, F.; Doumont, J.; Kalantari, L.; Huran, A. W.; Marques, M. A. L.; Blaha, P. Semilocal Exchange-Correlation Potentials for Solid-State Calculations: Current Status and Future Directions. *J Appl Phys* **2019**, *126* (11). https://doi.org/10.1063/1.5118863.

(62) Xiao, H.; Tahir-Kheli, J.; Goddard, W. A. Accurate Band Gaps for Semiconductors from Density Functional Theory. *J Phys Chem Lett* **2011**, *2* (3), 212–217. https://doi.org/10.1021/jz101565j.

(63) Wang, F.; Di Valentin, C.; Pacchioni, G. Electronic and Structural Properties of WO_3 : A Systematic Hybrid DFT Study. *The Journal of Physical*

View Article Online
DOI: 10.1039/D5NA00587F

Chemistry C **2011**, *115* (16), 8345–8353. https://doi.org/10.1021/jp201057m.

(64) Bolívar Marín, Y.; Alcalá Varilla, L. A.; González Ramirez, I. A. Comparative Study of the Effect of the Exchange-Correlation Functional on the Structural and Electronic Properties of Rutile. *J Phys Conf Ser* **2019**, *1386* (1), 012074. https://doi.org/10.1088/1742-6596/1386/1/012074.

(65) Makuła, P.; Pacia, M.; Macyk, W. How To Correctly Determine the Band Gap Energy of Modified Semiconductor Photocatalysts Based on UV–Vis Spectra. *J Phys Chem Lett* **2018**, *9* (23), 6814–6817. https://doi.org/10.1021/acs.jpclett.8b02892.

(66) Boles, M. A.; Ling, D.; Hyeon, T.; Talapin, D. V. The Surface Science of Nanocrystals. *Nat Mater* **2016**, *15* (2), 141–153. https://doi.org/10.1038/nmat4526.

(67) Reiss, P.; Protière, M.; Li, L. Core/Shell Semiconductor Nanocrystals. *Small* **2009**, *5* (2), 154–168. https://doi.org/10.1002/smll.200800841.

(68) Tappan, B. A.; Brutchey, R. L. Polymorphic Metastability in Colloidal Semiconductor Nanocrystals. *ChemNanoMat* **2020**, *6* (11), 1567–1588. https://doi.org/10.1002/cnma.202000406.

(69) Powell, A. E.; Hodges, J. M.; Schaak, R. E. Preserving Both Anion and Cation Sublattice Features during a Nanocrystal Cation-Exchange Reaction: Synthesis of Metastable Wurtzite-Type CoS and MnS. *J Am Chem Soc* **2016**, *138* (2), 471–474. https://doi.org/10.1021/jacs.5b10624.

(70) Momma, K.; Izumi, F. VESTA 3 for Three-Dimensional Visualization of Crystal, Volumetric and Morphology Data. *J Appl Crystallogr* **2011**, *44* (6), 1272–1276. https://doi.org/10.1107/S0021889811038970.

View Article Online
DOI: 10.1039/D5NA00587F

Solution-phase Synthesis and Characterization of Alkaline Earth Polysulfides as Colloidal Nanocrystals

Data Availability Statement

Additional data supporting the results in this article have been included as part of the ESI which includes additional pXRD data, XRF data, and TEM data, followed by a short supplementary discussion on precursor choices.